Proposal and Performance Evaluation of Microwave-driven In-tube Accelerator Concept

IEPC-2019-A577

Presented at the 36th International Electric Propulsion Conference
University of Vienna, Austria
September 15-20, 2019

Masayuki Takahashi*
Tohoku University, Sendai, Miyagi, 980-8579, Japan

A microwave-driven in-tube accelerator (MITA) concept was proposed to improve thrust performance and flight stability of a microwave rocket driven by an intense electromagnetic wave beam irradiated from the earth. The microwave beam, plasma, and shock wave propagations were numerically reproduced on the MITA system by conducting a two-dimensional axisymmetric simulation. More than one strong electric-field spot was created at the vehicle rear side because of a diffraction effect of the microwave. A dense plasma was formed at the vehicle rear because a quick electron-impact ionization occurred, and the plasma density increased by repeating the ionization. An overcritical plasma induced a quasi-standing wave at the vehicle rear because the microwave reflected by the dense plasma overlapped the incident microwave beam. A localized Joule heating occurred at the plasma front because of a plasma screening effect, which induced a strong shock wave. A momentum coupling coefficient became 100 N/MW in the MITA system because a positive pressure of the shock wave strongly interacted with the thruster wall.

Nomenclature

$\mathbf{B}$	= magnetic flux vector
C_M	= momentum coupling coefficient
D_{eff}	= effective diffusion coefficient
e	= elementary charge
$\mathbf{E}$	= electric field vector
$\mathbf{E}_f$, $\mathbf{F}_f$	= inviscid flux vector
$\tilde{\mathbf{E}}_f$, $\tilde{\mathbf{F}}_f$	= viscous flux vector
ϵ_0	= permittivity in vacuum
$\mathbf{H}$	= magnetic field vector
$\mathbf{H}_f$	= axisymmetric term
$\mathbf{J}$	= current density vector
λ	= microwave wavelength
m_e	= electron mass
n_e	= electron number density
ν_i	= electron-impact ionization frequency
ν_m	= elastic collision frequency
$\mathbf{Q}_f$	= conservative variable vector
r	= radial direction coordinate
$\mathbf{S}_f$	= energy source term

*Associate Professor, Department of Aerospace Engineering, mtakahashi@rhd.mech.tohoku.ac.jp

t = time
$\mathbf{v}$ = mean electron velocity
ξ = energy conversion rate
z = axial direction coordinate

I. Introduction

It is necessary to construct a low-cost launching system to open new fields of a space utilization such as space solar power supply system. Beamed-energy propulsion technique is one of the low-cost launching system using a laser or microwave beam. In beaming propulsion concept, an intense electromagnetic wave beam is irradiated from the beam oscillator established on the earth to flying rocket. The electromagnetic wave beam is focused inside the rocket nozzle using a focusing device equipped on the rocket, which induces a gas breakdown owing to an ionization process. A dense plasma is created inside the rocket nozzle by the gas breakdown process. An energy of the plasma increases by continuing irradiation of the electromagnetic wave beam, and neutral particles around the plasma are heated because an energy of the plasma is transferred to that of the neutral particles through a quenching collision process. The neutral gas having high temperature induces a strong shock wave inside the rocket nozzle. The rocket can obtain a propulsive force when a positive pressure of the shock wave interacts with the thruster wall. A negative pressure wave is also induced inside the rocket nozzle, but a net thrust becomes positive because a contribution of the positive pressure is larger than that of the negative pressure wave. After irradiation of a pulsed beam, the flying rocket has a breathing process to refresh air inside the nozzle. The next pulse is irradiated to the vehicle to create the plasma and shock wave, and a flying altitude of the vehicle increases with time by repeating these processes. Using the laser beam for the beaming flight is excellent in a directional energy transfer for a long distance,[1–5] but a construction cost of the laser oscillator tends to be higher than that of the microwave beam based on the past study for cost estimation.[6,7] Therefore, the beaming flight technique using the microwave, which called a microwave rocket, is focused on in this study.[8–16]

In the past experiments of the microwave rocket,[15,16] a flight demonstration of the microwave rocket was conducted using a high-power gyrotron to understand plasma physics driven by the microwave and measure thrust performance obtained from a shock wave interaction. The breakdown experiments by Oda *et al.* indicated that the thrust performance decreased with a decrease in an ambient pressure because a gas heating by the microwave became weaker, which meant that the beaming flight cannot be maintained at high altitudes. Moreover, a beam divergence in the microwave becomes a significant issue than the laser beam, which decreases the thrust performance at high altitudes because the rocket cannot capture the diverged microwave beam. It is necessary to overcome decreases in the thrust performance at high altitudes to achieve a high-transportation efficiency to the space. The breakdown experiment under a repetitive pulses operation was carried out to measure the thrust performance of the microwave rocket because an actual beaming flight is mainly sustained using the repetitive pulses.[16] During the repetitive pulses operation, it is necessary to irradiate the next pulse into the rocket nozzle after the plasma ignited by the previous pulse disappears. However, the repetitive pulses experiment indicated that the plasma inside the rocket nozzle did not disappear and the next pulse did not penetrate inside the rocket nozzle because the microwave beam was reflected by the previous plasma. Therefore, the thrust performance under the repetitive pulses decreased with time. This microwave reflection by the previous plasma should be avoided to maintain the repetitive pulses flight. It is necessary to separate the plasma exhausting line from beam incident line to avoid the plasma screening. In addition, a flight stability during the beaming flight is an issue to obtain a continuous thrust because the past experiment described that the vehicle deviated from the incident beam line and lost the propulsive force.[1–5,17] A microwave-driven in-tube acceleration (MITA) concept was proposed to improve the thrust performance at high altitudes, plasma screening at the repetitive pulses operation, and flight stability of the microwave rocket.[14] A concept of the MITA is considered by analogy to a laser-driven in-tube accelerator (LITA) concept proposed by Sasoh.[18,19] In the LITA, a vehicle was putted inside an acrylic resin tube and the thrust was generated by irradiating the laser pulses. However, a waveguide is used in the MITA, instead of an acrylic resin tube. A vehicle having a reflection mirror on the vehicle front is installed inside the waveguide in the MITA. Instead of the laser beam, the microwave beam is injected from the front side of the vehicle and reflected diagonally by the mirror equipped on the vehicle front. The microwave beam is reflected again by side walls of the waveguide, which is focused on at the rear side of the vehicle. The vehicle can obtain the thrust because the beam focusing at the vehicle rear generates the plasma and shock wave and an interaction between the shock wave and thruster wall is induced. The beam divergence can be avoided in the MITA because the microwave beam propagates inside the waveguide, and a long-distance wave transmission can be conducted. A pressure inside the waveguide can be sustained by injecting propellant gas, which means that the thrust performance of the vehicle can be maintained at high altitudes. A wave screening by the previous plasma does not occur under the repetitive pulses operation because the plasma is exhausted from the vehicle's rear side and the incident microwave beam comes from the front side. Therefore, the thrust performance does not decrease under the repetitive pulses operation. Moreover, a flight stability control is not required in the MITA because the vehicle is always guided by the waveguide.

In the previous work for the MITA, a one-dimensional (1D) plasma simulation was conducted to evaluate the thrust performance of the MITA.[14] However, the electromagnetic wave, plasma, and shock wave propagations in the MITA have a multi-dimensional structure. Therefore, it is necessary to conduct a multi-dimensional simulation to reproduce the plasma and shock wave propagations around the vehicle in the MITA. We assume that the electromagnetic wave injection having the 2D axisymmetric mode in this study; therefore, a simulation code, which reproduces the 2D axisymmetric electromagnetic wave, plasma, and shock wave propagations, was constructed. A momentum coupling coefficient of the MITA, which is thrust efficiency against the input beam power, was finally evaluated by integrating the pressure and viscous force on the vehicle surface.

II. Numerical Methods

A. Electromagnetic wave propagation

The following 2D axisymmetric Maxwell's equations are numerically integrated, by utilizing a finite-difference time-domain (FDTD) method, to reproduce the electromagnetic wave propagation with 2D axisymmetric mode inside the waveguide:

$$\nabla \times \mathbf{E} = -\frac{\partial \mathbf{B}}{\partial t}, \tag{1}$$

$$\nabla \times \mathbf{H} = \epsilon_0 \frac{\partial \mathbf{E}}{\partial t} + \mathbf{J}. \tag{2}$$

The time step for integration is determined by Courant-Friedrichs-Lewy (CFL) condition for a light speed. A current density vector $\mathbf{J}$ is set as zero when only the FDTD simulation is conducted to check the electromagnetic wave reflection and focusing inside the waveguide. However, a coupling calculation between the electromagnetic wave and plasma is required because an interaction between the plasma and electromagnetic wave plays an important role on the pattern formation of the microwave plasma in the MITA. The current density vector $\mathbf{J}$ is calculated by a 2D axisymmetric plasma fluid model, which is fed back to the 2D axisymmetric Maxwell's equations to reproduce the interaction between the plasma propagation and electromagnetic wave.

B. Fluid modeling for plasma transport

It is necessary to model the charged-particle transport and collisional reaction to reproduce the plasma propagation physics in the MITA. The 2D axisymmetric plasma fluid model based on a quasi-neutral assumption, which is proposed by Boeuf,[20] is used here to capture the plasma behavior inside the waveguide. The following electron diffusion equation having a source term for an electron-impact ionization process is numerically integrated:

$$\frac{\partial n_e}{\partial t} - D_{\mathrm{eff}} \left(\frac{\partial^2 n_e}{\partial z^2} + \frac{\partial^2 n_e}{\partial r^2} \right) - \frac{D_{\mathrm{eff}}}{r} \frac{\partial n_e}{\partial r} = n_e \nu_e. \tag{3}$$

The electron diffusion flux is evaluated by the second-order central difference scheme. The time integration is conducted by the first-order Euler explicit method. The integration time step of the diffusion equation is set as one-period of the microwave oscillation. The electron velocity is updated by solving the following equations of motion for the electron:

$$\frac{\partial \mathbf{v}}{\partial t} = -\frac{e\mathbf{E}}{m_e} - \nu_m \mathbf{v}. \tag{4}$$

The Lorentz force effect is ignored here because its contribution is much smaller than the electric field. The time integration of the equations of motion is conducted by the first-order Euler explicit method. The integration time step is same as that of the FDTD simulation. The current density vector is evaluated as $\mathbf{J} = -en_e\mathbf{v}$ in the 2D axisymmetric plasma fluid model, which is fed back to Eq. (2) to reproduce the wave-plasma interaction.

C. Shock wave simulation

The dense plasma is generated by the electron-impact ionization process when the microwave is focused by the mirror. A rapid heating for the neutral particles is then obtained by continuing a microwave irradiation because energy of the plasma is transferred to that of the neutrals particle through a quenching collision process. A strong shock wave is induced from the heating spot, which is numerically reproduced by solving the following 2D axisymmetric Navier-Stokes (NS) equation:

$$\frac{\partial \mathbf{Q}_f}{\partial t} + \frac{\partial (\mathbf{E}_f - \tilde{\mathbf{E}}_f)}{\partial z} + \frac{\partial (\mathbf{F}_f - \tilde{\mathbf{F}}_f)}{\partial r} + \mathbf{H}_f = \mathbf{S}_f. \tag{5}$$

Discretization is performed in a cell-centered finite-volume method.[21] The AUSM-DV method with the entropy fix[22] is employed to evaluate the inviscid fluxes with the second-order monotonic upwind scheme for conservation laws (MUSCL) method.[23] In the MUSCL method, the characteristic variables are chosen as interpolation quantities, and they use the minmod limiter to fulfill the total variation diminishing condition. The viscous fluxes are evaluated by the second-order central difference. Numerical flux is evaluated using a local rotation matrix at the cell interface to introduce a general curvilinear coordinate.[24,25] Time integration is performed using the first-order explicit Euler method. The Spalart-Allmaras one-equation model is introduced to reproduce the turbulence flow by assuming the whole surface turbulence.[26] An energy source term by Joule heating is evaluated by $\mathbf{J} \cdot \mathbf{E}$ in the plasma-FDTD coupling simulation, which is used to describe the energy source term in the NS equation. The energy source term is modeled as $\mathbf{S}_f = \xi \mathbf{J} \cdot \mathbf{E}$ by considering the energy conversion rate from the plasma to neutral particle ξ as 15%. The time step for the neutral fluid model is determined by CFL condition for the compression, expansion, and entropy waves propagation. The temporal integration for the FDTD-plasma model is conducted for several times during one time step for the fluid model because the time step determined by the FDTD-plasma model is much smaller than that of the NS simulation. The transport coefficients of the plasma may change when the neutral gas density changes owing to the compression and expansion processes, but the change in the transport coefficients is ignored in this simulation for simplification.

III. Simulation Conditions

A. FDTD-plasma coupling simulation

A radius of the waveguide is set as 2.4 cm, following the tube radius of the LITA system proposed by Sasoh.[18,19] A triangular vehicle which has a same shape as the LITA is installed inside the waveguide. A mirror is equipped on the vehicle front to reflect the microwave beam injected from the vehicle front. After wave reflection by the front mirror, the microwave beam is reflected again by the side wall of the waveguide. The microwave beam is then focused at the rear side of the vehicle to generate the plasma spot and shock wave. In the computational domain, the microwave source is set at the left boundary. The total-field scattered-field implementation is applied at the injection side. The beam frequency is set as 110 GHz, following Hidaka's experiment.[27] An electric field intensity is selected as 0.8 MV/m to do only the FDTD simulation for checking the electromagnetic wave propagation process inside the waveguide. However, when the thrust performance is evaluated by conducting the FDTD-plasma coupling simulation, the electric field intensity is set as 8 MV/m to save a computational time. The TM_{01} mode, which has the 2D axisymmetric mode, is injected inside the waveguide. The Mur's absorbing boundary is set at the boundary of the microwave injection side.[28] The PML absorbing boundary is set at the downstream boundary because an oblique propagation to the boundary is remarkable. The z-directing electric field is set as 0 on the waveguide wall. The electric field is set as 0 on the vehicle surface. The gas inside the waveguide is set as pure nitrogen. The gas pressure is set as 100 kPa, and gas temperature is set as 300 K. The electron-impact ionization frequency, electron mobility, diffusion coefficient, and elastic collision frequency in the plasma fluid model are evaluated from a particle-in-cell (PIC) simulation coupled with Monte Calro collision (MCC) model.[10] Based on the PIC-MCC simulation, a data table for the transport coefficients is made against the root-mean-square (rms) electric field $E_{\rm rms}$. $E_{\rm rms}$ is evaluated by an integration for one-microwave period in the plasma-FDTD simulation, which is used to evaluate the local transportation coefficients by interpolation on the data table made by the PIC-MCC model.

B. Computational fluid dynamics simulation

The energy source term in the energy conservation equation $\mathbf{S}_f$ is modeled based on the Joule heating rate evaluated in the plasma-FDTD coupling simulation. The mass, momentum, and energy conservation equations for the neutral fluid are numerically integrated together with the plasma-FDTD coupling integration, while obtaining the Joule heating rate from the plasma-FDTD coupling simulation. The non-slip boundary condition is applied on the walls of the thruster and waveguide. The axisymmetric boundary condition is set at the axis of the simulation domain. The zeroth-order extrapolation is adapted on the other boundaries. A sufficiently large simulation domain is utilized to avoid a non-physical reflection from the outer boundaries. An axial thrust is evaluated by integrating the pressure and viscous forces on the vehicle surface. The momentum coupling coefficient is calculated based on the axial thrust.

IV. Results

A. Wave reflection and focusing processes

The microwave having a 110-GHz frequency and a 0.8-MV/m intensity is injected from the left to right boundaries in the computational domain to check a quality of beam focusing. The current density term is not fed back to the Maxwell's equations and the plasma-FDTD coupling simulation is not conducted here. Additionally, the neutral fluid equation is not integrated to save the computational cost. The microwave beam is reflected by the mirror equipped on the vehicle front (Fig. 1(a)). After the wave reflection by the front mirror, the microwave beam is successfully focused at the rear side of the vehicle because of reflection by the side wall. More than one high-intensity spot is created at the rear side of the vehicle because of an effect of wave diffraction (Fig. 1(b)). The diffraction effect is determined by a ratio of the microwave wavelength and radius of the waveguide. It is better to obtain a single focal spot to get the much stronger electric field at the focal spot. A single focal spot can be obtained if the wavelength is decreased or the waveguide radius is increased because the diffraction effect becomes weaker.

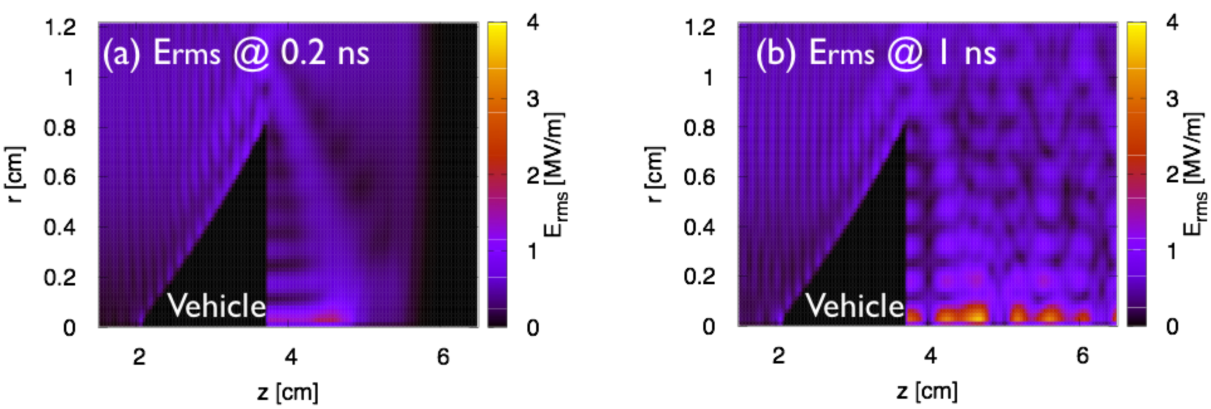

Figure 1. Root-mean-square electric field $E_{\rm rms}$.

B. Plasma and shock wave propagations

The microwave of a 110-GHz frequency and an 8-MV/m intensity is injected from the left to right boundaries to conduct the plasma-FDTD coupling simulation. The current density term in the Maxwell's equations is added in this section, and the NS equation is integrated together with the plasma-FDTD coupling model to capture the shock wave. The beam focusing is obtained at the vehicle rear side because of the beam reflections by the mirror, which creates the enhanced electric field spots. An electron-impact ionization is rapidly induced at the strong electric field spots because the electrons are heated by the electric field. The plasma density increases at the focal spots and exceeds the critical value for wave reflection. The incident microwave beam is reflected by the overcritical plasma at the vehicle rear side. A quasi-standing wave is formed at the vehicle rear side because the microwave reflected by the overcritical plasma overlaps the incident microwave beam. The rapid ionization occurs at an antinode of the standing wave when the electron diffuses from the bulk region to wave antinode. A new dense plasma spot is then created by the rapid ionization at the antinode, which drives the plasma front toward the microwave source. A $\lambda/4$ structure of the microwave plasma appears at the vehicle rear side because of the effect of the standing wave. The microwave penetrates only the plasma front owing to the reflection effect by the overcritical plasma, which induces the strong Joule heating region at the plasma front. This strong heating increases energy of the neutral particle rapidly through a quenching process, which drives a strong shock wave propagation from the vehicle rear (Fig. 2). A positive thrust is generated when a positive pressure of the shock wave interacts with the thruster wall, but a negative thrust is generated after the positive thrust because an negative pressure wave interacts with the thruster wall. However, a net thrust becomes positive value because the negative pressure wave decays rapidly. A momentum coupling coefficient C_M is evaluated from a temporal integration for the thrust, which indicates that C_M becomes 100 N/MW. There is a possibility that the MITA system is better than the LITA system based on the laser beam because C_M is comparable level with that of the LITA and a construction cost of the microwave source can be lower than the laser oscillation.

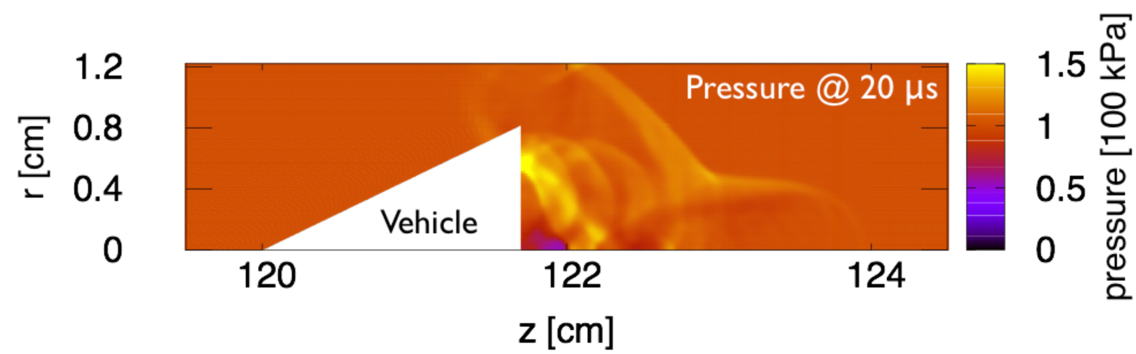

Figure 2. Pressure distribution around the vehicle at 20 μs.

V. Conclusion

The 2D axisymmetric simulation including the electromagnetic wave, plasma, and shock wave propagations was conducted in this paper to capture the microwave, plasma, and pressure wave structures in the MITA system. The microwave focusing was successfully achieved at the vehicle rear side through the mirror reflection. The strong ionization was obtained at the vehicle rear because of the enhanced electric field of the focused microwave. The plasma front propagated toward the microwave source by repeating the wave reflection, plasma transport, and ionization. A localized Joule heating region was created at the plasma front because the microwave penetrated only the plasma front. The shock wave was then driven by Joule heating, which interacted with the thruster wall inside the waveguide. The momentum coupling coefficient became 100 N/MW in the MITA system because of an interaction with a positive pressure of the shock wave. In the future work, optimal parameters will be searched to maximize the thrust performance of the MITA.

Acknowledgments

The fluid simulations in this work were performed on a FUJITSU Server PRIMERGY CX2550M4 at the Advanced Fluid Information Research Center, Institute of Fluid Science, Tohoku University and a FUJITSU PRIMEHPC FX100 at the Japan Aerospace Exploration Agency. This work was supported by JSPS KAKENHI Grant Number JP17K14872.

References

[1]Takahashi, M. and Ohnishi, N., "Beam Riding Performance of Asymmetrically Propelled Laser Vehicle," *AIAA Journal*, Vol. 50, 2011, pp. 2600–2608.

[2]Takahashi, M. and Ohnishi, N., " Fluid-orbit Coupling Calculation for Flight Analysis of Impulsively Driven Laser Vehicle," *Journal of Physics: Conference Series*, Vol. 454, 2013, 012004.

[3]Takahashi, M. and Ohnishi, N., "Beaming Flight of Repetitive-pulse Powered Vehicle for Satellite Launch," *Transactions of Japan Society for Aeronautical and Space Sciences*, Vol. 12, 2014, pp. Pb_97–Pb_102.

[4]Takahashi, M. and Ohnishi, N., "Theoretical and Numerical Studies of Dynamic Scaling of Six-degree-of-freedom Laser Propulsion Vehicle," *International Journal of Aerospace Engineering*, Vol. 2015, 2015, 801371.

[5]Takahashi, M. and Ohnishi, N., "Beam-riding Flight of a Laser-Propulsion Vehicle Using Actively Controlled Pulse," *Journal of Propulsion and Power*, Vol. 32, 2016, pp. 237–250.

[6]Fukunari, M., Arnault, A., Yamaguchi, T., and Komurasaki, K., "Design of a Millimeter-Wave Concentrator for Beam Reception in High-Power Wireless Power Transfer," *Applied Optics*, Vol. 38, 2016, pp. 176–190.

[7]Fukunari, M., Wongsuryrat, N., Yamaguchi, T., Nakamura, Y., Komurasaki, K., and Koizumi, H., "Design of a Millimeter-Wave Concentrator for Beam Reception in High-Power Wireless Power Transfer," *Journal of Infrared Millimeter and Terahertz Waves*, Vol. 38, 2016, pp. 176–190.

[8]Takahashi, M. and Ohnishi, N., "Plasma Filamentation and Shock Wave Enhancement in Microwave Rockets by Combining Low-Frequency Microwaves with External Magnetic Field," *Journal of Applied Physics*, Vol. 120, 2016, 063303.

[9]Takahashi, M. and Ohnishi, N., "Computational Studies for Plasma Filamentation by Magnetic Field in Atmospheric Microwave Discharge," *Applied Physics Letters*, Vol. 105, 2014, 223504.

[10]Takahashi, M. and Ohnishi, N., "Numerical Study of Breakdown Pattern Induced by Intense Microwave under Nitrogen and Argon Gases," *Japanese Journal of Applied Physics*, Vol. 55, 2016, 07LD02.

[11]Takahashi, M. and Ohnishi, N., "Open-front Approach of a Microwave Rocket Sustained by a Resonant Magnetic Field," *Journal of Propulsion and Power*, Vol. 34, 2018, pp. 762–771.

[12]Takahashi, M. and Ohnishi, N., "Gas-Species-Dependence of Microwave Plasma Propagation under External Magnetic Field," *Journal of Applied Physics*, Vol. 124, 2018, 173301.

[13]Takahashi, M. and Ohnishi, N., "Gas Propellant Dependency of Plasma Structure and Thrust Performance of Microwave Rocket," *Journal of Applied Physics*, Vol. 125, 2019, 163303.

[14]Takahashi, M. and Ohnishi, N., "Numerical Study of Discharge and Thrust Generation in a Microwave Rocket," AIAA Paper 2019-1242, 2019.

[15]Oda, Y., Komurasaki, K., Takahashi, K., Kasugai, A., and Sakamoto, K., "Plasma Generation Using High-Power Millimeter-Wave Beam and Its Application for Thrust Generation," *Journal of Applied Physics*, Vol. 100, 2006, 113307.

[16]Oda, Y., Shibata, T., Komurasaki, K., Takahashi, K., Kasugai, A., and Sakamoto, K., "Thrust Performance of a Microwave Rocket Under Repetitive-Pulse Operation," *Journal of Propulsion and Power*, Vol. 25, 2009, pp. 118–122.

[17]Ballard, C. G., Anderson, K. S., and Myrabo, L. N., "Flight Dynamics and Simulation of Laser Propelled Lightcraft," *Journal of Computational Nonlinear Dynamics*, Vol. 4, 2009, 041005.

[18]Sasoh, A., Urabe, N., Kim, S. S. M., and Jeung, L. S., "Impulse-Scaling in a Laser-Driven In-Tube Accelerator," *Applied Physics A*, Vol. 77, 2003, pp. 349–352.

[19]Sasoh, A., "Laser-Driven In-Tube Accelerator," *Review of Scientific Instruments*, Vol. 72, 2001, pp. 1893–1898.

[20]Boeuf, J. P., Chaudhury, B., and Zhu, G. Q., "Theory and Modeling of Self-Organization and Propagation of Filamentary Plasma Arrays in Microwave Breakdown at Atmospheric Pressure," *Physical Review Letters*, Vol. 104, 2010, 015002.

[21]Hirsch, C., *Numerical Computation of Internal and External Flows*, Vol. 1, New York: John Wiley and Sons, 1984, pp. 237–266.

[22]Wada, Y. and Liou, M. S., "A Flux Splitting Scheme with High-Resolution and Robustness for Discontinuities," AIAA Paper 2006-1358, 2006.

[23]van Leer, B., "Toward the Ultimate Conservative Difference Scheme V, A Second-Order Sequel to Godunov's Method," *Journal of Computational Physics*, Vol. 32, 1979, pp. 101–136.

[24]Toro, E. F., *Riemann Solvers and Numerical Methods for Fluid Dynamics*, 3rd ed., Springer Press, New York, 2010, pp. 574–584.

[25]Toro, E. F. and Clarke, J. F., *Numerical Methods for Wave Propagation*, Kluwer Academic Publishers, London, 1998, pp. 89–91.

[26]Spalart, P. R. and Allmaras, S. R., "A One-Equation Turbulence Model for Aerodynamic Flows," AIAA Paper 92-0439, 1992.

[27]Hidaka, Y., Choi, E. M., Mastovsky, I., Shapiro, M. A., Sirigiri, J. R., and Temkin, R. J., "Observation of Large Arrays of Plasma Filaments in Air Breakdown," *Physical Review Letters*, Vol. 100, 2008, 035003.

[28]Mur, G., "Absorbing Boundary Condition for the Finite-Difference Approximation of the Time-Domain Electromagnetic-Field Equations," *IEEE Transactions on Electromagnetic Compatibility*, Vol. EMC-23, 1981, pp. 377–382.